Structure-Aware Contrastive Learning with Fine-Grained Binding Representations for Drug Discovery

Jing Lan[*1], Hexiao Ding[*1], Hongzhao Chen[*1], Yufeng Jiang[1], Nga-Chun Ng[1,2]
Gwing Kei Yip[1,3], Gerald W.Y. Cheng[1], Yunlin Mao[1], Jing Cai[1], Liang-ting Lin[1], Jung Sun Yoo[#1]
[1]Department of Health Technology and Informatics, The Hong Kong Polytechnic University
[2]Department of Nuclear Medicine and PET, Hong Kong Sanatorium and Hospital
[3]Nulcear Medicine Unit, Department of Diagnostic and Interventional Radiology, Queen Elizabeth Hospital
Hong Kong SAR, China
Emails: {jing-hti.lan, hexiao.ding, hongzhao.chen, yufeng.jiang, yunlin.mao}@connect.polyu.hk
{wai-yeung.cheng, jing.cai, ltlin, jungsun.yoo}@polyu.edu.hk
{sam.nc.ng}@hksh.com, {gwinky.yip}@ha.org.hk

***Abstract*—Accurate identification of drug–target interactions (DTI) remains a central challenge in computational pharmacology, where sequence-based methods offer scalability. This work introduces a sequence-based drug–target interaction framework that integrates structural priors into protein representations while maintaining high-throughput screening capability. Evaluated across multiple benchmarks, the model achieves state-of-the-art performance on Human and BioSNAP datasets and remains competitive on BindingDB. In virtual screening tasks, it surpasses prior methods on LIT-PCBA, yielding substantial gains in AUROC and BEDROC. Ablation studies confirm the critical role of learned aggregation, bilinear attention, and contrastive alignment in enhancing predictive robustness. Embedding visualizations reveal improved spatial correspondence with known binding pockets and highlight interpretable attention patterns over ligand–residue contacts. These results validate the framework's utility for scalable and structure-aware DTI prediction. Code is available at https://github.com/1anj/SaBAN-DTI.**

***Index Terms*—Drug discovery, Drug-target interactions, Attention network, Contrastive learning**

I. Introduction

Predicting compound–protein binding potential is essential for drug discovery. However, binding affinity alone does not capture the full pharmacological features because location of binding, conformational adaptation, and kinetic stability shape efficacy and selectivity [1]. Physics-based free energy methods can fully recover these factors yet remain costly at the screening scale [2]. Fast geometric docking has improved throughput, but the practical gate in many pipelines is still the presence or absence of interaction. Therefore, drug-target interaction (DTI) prediction functions as a rapid prescreen that precedes pose refinement and affinity estimation.

Public datasets and benchmarks have advanced DTI research by enabling model development and exposing persistent gaps. ChEMBL [3] provides extensive bioactivity annotations across diverse targets and modalities, BioLiP2 [4] integrates structure-based evidence for biologically relevant interactions. Moreover, BindingDB [5] continues to expand with curated binding measurements from literature and patents. Despite these resources, a considerable portion of interaction evidence remains embedded in unstructured text and requires specialized extraction methods such as DrugProt [6] to produce machine-readable data. These approaches enable efficient training and provide interpretable attention-based explanations. However, they remain sensitive to dataset split strategies and often make limited use of explicit pocket level geometric information.

We present a sequence-based DTI framework that injects structural signals while preserving screening speed and accuracy. Proteins are represented using a structure-aware vocabulary that pairs each residue token with a compact descriptor of local geometry. A large protein language model is pretrained on sequences annotated with these descriptors, enabling the encoder to learn structural context while operating on plain sequence inputs. Encoding small molecules with SELFIES guarantees validity and preserves chemical semantics [7]. Both drug and protein encoders employ a patch-based convolutional trunk that maintains input resolution and supplies token features to attention-based aggregation, which yields an interpretable importance map over patches [8]. A contrastive learning objective aligns drug and protein embeddings by drawing together regions corresponding to true binding interfaces. Our main contributions are as follows:

1) Propose a structure-aware protein sequence representation that augments each residue token with a compact local-geometry descriptor, enabling structural context learning from plain sequences.
2) Introduce an attention-based aggregation module that preserves resolution, focuses on binding-relevant regions,

*Co-first author
#Corresponding author

and produces interpretable importance maps.

3) Deliver a DTI prediction framework that outperforms existing baselines in accuracy and speed, supporting large-scale virtual screening for drug discovery.

II. Methodology

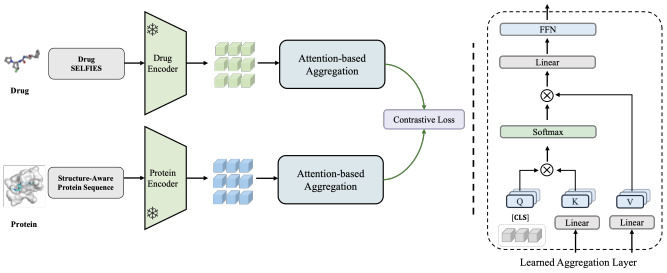

Fig. 1: **Model Architecture.** Our framework encodes drug and protein sequences independently using frozen pre-trained models. The resulting embeddings are aggregated through an attention-based module and optimized via a contrastive learning objective. Cosine similarity between drug and protein representations is used to compute interaction probabilities, which support discriminative prediction of drug-target interactions and enable large-scale virtual screening.

A. Representations of Drugs and Protein Targets

1) Drug and protein encoders: As shown in Figure 1, the initial inputs of our model are string-based representations of drugs and proteins. For a protein sequence P, we adopt the *structure-aware vocabulary* [8], where each residue is replaced by one of 441 tokens that couple amino acids with 3-D geometric features. This design alleviates the lack of explicit structural information in amino acid sequences. For a drug sequence D, we employ SELFIES [7], a robust chemical string representation where every valid string representation can be unambiguously decoded into a chemically valid molecular graph, thereby avoiding invalid structures that may arise from SMILES.

Two frozen pre-trained encoders are employed to transform input sequences into representations. Protein sequences are encoded by Saport [8], which jointly models amino acid tokens and structural features to produce embeddings $\mathbf{P}$. Drug SELFIES sequences are processed by SELFormer [9], yielding embeddings $\mathbf{D}$. These embeddings capture cross-modal semantics relevant to molecular binding. The modular framework supports substitution with alternative language models, such as ESM-2 [10] for proteins or ChemBERTa-2 [11] for molecules.

2) Attention-based pooling: Local binding pockets contain key drug-target interaction signals, which can be diluted when subjected to average pooling through a learned aggregation layer. To preserve fine-grained contact features encoded via self-attention, token-level embeddings are aggregated using an attention-based pooling module adapted from transformer architectures [12].

Formally, let $\mathbf{H} \in \mathbb{R}^{n\times d}$ denote the sequence of n token embeddings with hidden size d. A learnable class token $\mathbf{q} \in \mathbb{R}^{1\times d}$ serves as the query against projected keys and values:

$$\mathbf{K} = \mathbf{H}\mathbf{W}_K, \quad \mathbf{V} = \mathbf{H}\mathbf{W}_V, \qquad \mathbf{W}_K, \mathbf{W}_V \in \mathbb{R}^{d\times d}. \quad (1)$$

The attention weights and pooled embedding are computed as

$$\boldsymbol{\alpha} = \mathrm{softmax}\Big(\frac{\mathbf{q}\mathbf{K}^\top}{\sqrt{d}}\Big) \in \mathbb{R}^{1\times n}, \qquad \tilde{\mathbf{z}} = \boldsymbol{\alpha}\mathbf{V} \in \mathbb{R}^{1\times d}. \quad (2)$$

A residual connection with the class token, followed by a lightweight feed-forward network (FFN), produces the final representation:

$$\mathbf{h} = \mathrm{FFN}(\tilde{\mathbf{z}} + \mathbf{q}) \in \mathbb{R}^{1\times d}. \quad (3)$$

This formulation concentrates the aggregation into a single-head attention block, ensuring interpretability of how token-level signals contribute to the final representation.

B. Contrastive Learning for Drug-Target Interactions

We aligned drug and protein embeddings in a shared latent space via a symmetric contrastive objective. Given N drug–target pairs, pooled embeddings $\mathbf{h}_d^i$ and $\mathbf{h}_t^i$ are projected to co-embeddings

$$\mathbf{Z}_d^i = C_d(\mathbf{h}_d^i), \qquad \mathbf{Z}_t^i = C_t(\mathbf{h}_t^i), \quad (4)$$

and normalized as $\hat{\mathbf{Z}}_d^i = \mathbf{Z}_d^i/\|\mathbf{Z}_d^i\|$, $\hat{\mathbf{Z}}_t^i = \mathbf{Z}_t^i/\|\mathbf{Z}_t^i\|$. Cosine similarity is thus given by the inner product $\hat{\mathbf{Z}}_d^i \cdot \hat{\mathbf{Z}}_t^i$.

For drug-to-target alignment, the probability of a correct match is

$$p(t = i \mid d = i) = \frac{\exp\Big(\alpha\, \hat{\mathbf{Z}}_d^i \cdot \hat{\mathbf{Z}}_t^i\Big)}{\sum_{j=1}^N \exp\Big(\alpha\, \hat{\mathbf{Z}}_d^i \cdot \hat{\mathbf{Z}}_t^j\Big)}, \quad (5)$$

with analogous formulation for target-to-drug. The overall loss is the symmetric InfoNCE:

$$\mathcal{L}_{\mathrm{con}} = -\tfrac{1}{2N}\sum_{i=1}^{N}\big[\log p(t = i \mid d = i) + \log p(d = i \mid t = i)\big]. \quad (6)$$

This training objective pulls embeddings of interacting pairs together and pushes non-interacting pairs apart, yielding discriminative and transferable representations for DTI prediction and virtual screening.

C. Bilinear Attention for Interaction Representation

A bilinear attention network (BAN) captures token-level interactions between drug and target. Given token embeddings $\mathbf{H}_d \in \mathbb{R}^{n_d\times d}$ and $\mathbf{H}_t \in \mathbb{R}^{n_t\times d}$, we first obtain projected features $\mathbf{D} = \phi(\mathbf{H}_d\mathbf{U})$ and $\mathbf{T} = \phi(\mathbf{H}_t\mathbf{V})$ with $\mathbf{U}, \mathbf{V} \in \mathbb{R}^{d\times r}$ and pointwise nonlinearity ϕ.

$$\mathbf{A} = \mathrm{softmax}\big(\mathbf{D}\mathbf{T}^\top\big) \in \mathbb{R}^{n_d\times n_t} \quad (7)$$

$$\mathbf{f} = \sum_{i=1}^{n_d}\Big(\mathbf{D}_i \odot (\mathbf{A}\mathbf{T})_i\Big) \in \mathbb{R}^r \quad (8)$$

A single-head BAN uses (7)–(8), and multi-glimpse BAN repeats them with separate $(\mathbf{U}_g, \mathbf{V}_g)$ and concatenates $\mathbf{f}_g$. Finally, an MLP maps $\mathbf{f}$ to the interaction probability.

TABLE I: Experimental dataset statistics

Dataset	# Drugs	# Proteins	# Interactions
Drug-Target Interaction			
BindingDB [5]	14,643	2,623	49,199
BioSNAP [14]	4,510	2,181	27,464
Human [15], [16]	2,726	2,001	6,728
Drug Virtual Screening			
LIT-PCBA [17]	415,225	15	–

Notes. BioSNAP and Human sets originate from Huang et al. (2021) [23] and Liu et al. (2015) [15], respectively. The BindingDB subset is a low-bias version compiled from the original database: (*i*) only pairs with $IC_{50} < 100\,nM$ (positive) or $IC_{50} > 10\,000\,nM$ (negative) are kept, yielding a 100-fold margin to suppress label noise; (*ii*) drugs exhibiting exclusively positive or negative pairs are removed to mitigate ligand-level bias.

III. Experiments

A. Datasets and Baselines

The framework is assessed using DTI prediction and virtual screening. Following the DrugBAN [13] setting, BindingDB [5], BioSNAP [14], and Human [15], [16] datasets are employed for DTI prediction, where each dataset is split into training, validation, and test sets with a 7:1:2 ratio, and evaluated using 5-fold cross-validation ($k = 5$). Virtual screening is conducted on the LIT-PCBA benchmark [17]. Dataset statistics are reported in Table I.

The framework is evaluated against classical machine learning (ML) and deep learning (DL) baselines. Classical ML models include SVM and random forest trained on ECFP4 [18] and PSC descriptors [19]. DL baselines cover GNN-CPI [20], DeepConv-DTI [21], GraphDTA [22], MolTrans [23], and DrugBAN [13]. For virtual screening, comparisons include Surflex [24], Glide-SP [25], Planet [26], BigBind [27], and DrugCLIP [28]. Also, DrugCLIP is included as a contrastive learning baseline.

B. Implementation Details

Training utilizes the AdamW optimizer with a learning rate of 5×10^{-5}, weight decay of 1×10^{-4}, and batch size of 64. Early stopping is applied after 20 epochs without improvement, with a maximum of 200 epochs. Drug and protein encoders generate embeddings of size 768 and 1280, respectively, which are linearly mapped to a shared 1024-dimensional latent space. Interaction modeling is performed using a bilinear attention module with 8 learnable heads. A dropout rate of 0.05 is applied throughout the network.

IV. Results & Discussion

A. Performance on DTI

Across three DTI datasets, the model achieves state-of-the-art results on Human and BioSNAP benchmarks. On BindingDB, performance aligns closely with DrugBAN and remains competitive with leading baselines. These results demonstrate consistent generalization and validate the effectiveness of the proposed architecture, as shown in Table II.

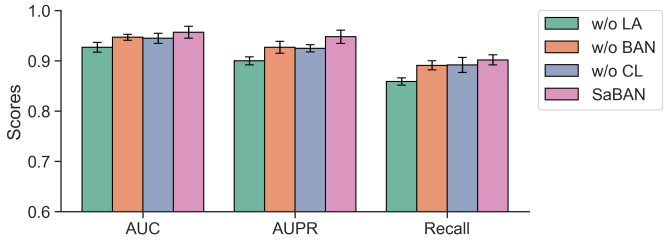

Fig. 2: Comparison between SaBAN and its variants on BindingDB dataset

B. Performance on Virtual Screening

On the LIT-PCBA benchmark for virtual screening, the proposed method outperforms the previous state-of-the-art, DrugCLIP, as shown in Table III. SaBAN achieves an AUROC of 68.16%, yielding a 10.99% absolute improvement. For early recognition, SaBAN attains a BEDROC of 13.35%, exceeding DrugCLIP by more than twofold.

C. Ablation Study

To quantify the contribution of each module, we conducted ablation experiments by removing the learned aggregation layer (LA), the bilinear attention network (BAN), and the contrastive learning (CL) components. As shown in Figure 2, removing LA results in the largest performance degradation across all metrics. Excluding BAN or CL also leads to noticeable declines, confirming that both interaction modeling and representation regularization are important for robustness.

D. Visualization

We visualize the embedding distribution for the CYP3A4 target and its attention profile to interpret the representations. Figure 3(a) shows the T-SNE projection, where SaBAN produces embeddings with positive samples positioned closer to the binding pocket than DrugCLIP, indicating improved structural correspondence. Figure 3(b) displays the ligand-level attention weights, concentrating on functional residues within the pocket and providing evidence of model interpretability.

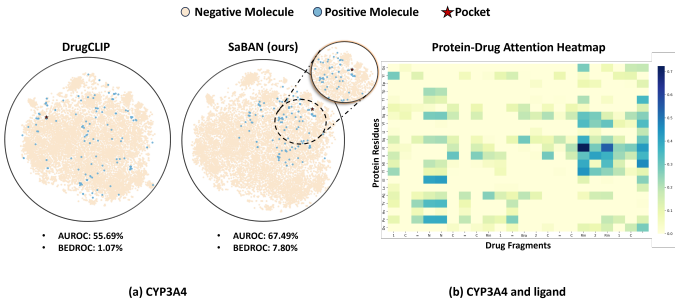

Fig. 3: Visualization of feature distributions for the target CYP3A4 (a) using DrugCLIP and SaBAN models and the attention map (b) of its ligand

TABLE II: Performance comparison of DTI prediction methods on BindingDB, Human, BioSNAP datasets

Method	BindingDB			Human		BioSNAP		
	AUROC ↑	AUPRC ↑	Accuracy ↑	AUROC ↑	AUPRC ↑	AUROC ↑	AUPRC ↑	Accuracy ↑
SVM [29]	.939 ± .001	.928 ± .002	.825 ± .004	.940 ± .006	.920 ± .009	.862 ± .007	.864 ± .004	.777 ± .011
RF [30]	.942 ± .011	.921 ± .016	.880 ± .012	.952 ± .011	.953 ± .010	.860 ± .005	.886 ± .005	.804 ± .005
DeepConv-DTI [21]	.945 ± .002	.925 ± .005	.882 ± .007	.980 ± .002	.981 ± .002	.886 ± .006	.890 ± .006	.805 ± .009
GraphDTA [22]	.951 ± .002	.934 ± .002	.888 ± .005	.981 ± .001	.982 ± .002	.887 ± .008	.890 ± .007	.800 ± .007
MolTrans [23]	.952 ± .002	.936 ± .001	.887 ± .006	.980 ± .002	.978 ± .003	.895 ± .004	.897 ± .005	.825 ± .010
DrugBAN [13]	.960 ± .001	**.948 ± .002**	**.904 ± .004**	.982 ± .002	.980 ± .003	.903 ± .005	.902 ± .004	.834 ± .008
SiamDTI [31]	**.961 ± .002**	.945 ± .002	.890 ± .006	.970 ± .002	.969 ± .003	.912 ± .005	.910 ± .003	.855 ± .004
SaBAN (Ours)	.957 ± .002	**.948 ± .001**	.902 ± .003	**.983 ± .003**	**.984 ± .006**	**.930 ± .003**	**.929 ± .002**	**.858 ± .006**

Notes. Best values are in **bold**; Second-best are underlined; Evaluation metrics include Area Under the Receiver Operating Characteristic Curve (AUROC), Area Under the Precision-Recall Curve (AUPRC), and accuracy. Model selection was based on the highest validation AUROC, and final results were averaged over five-fold cross-validation.

TABLE III: Performance comparison on LIT-PCBA benchmark

Method	AUROC (%) ↑	BEDROC (%) ↑	EF ↑		
			0.5%	1%	5%
Surflex [24]	51.47	-	-	2.50	-
Glide-SP [25]	53.15	4.00	3.17	3.41	2.01
Planet [26]	57.31	-	4.64	3.87	2.43
GNINA [32]	60.93	5.40	-	4.63	-
DeepDTA [33]	56.27	2.53	-	1.47	-
BigBind [27]	60.80	-	-	3.82	-
DrugCLIP [28]	57.17	6.23	8.56	5.51	2.27
SaBAN (Ours)	**68.16**	**13.35**	**9.17**	**6.33**	**3.36**

Notes. Best values are in **bold**; second-best are underlined. For virtual screening, the Boltzmann-Enhanced Discrimination of Receiver Operating Characteristic (BEDROC) and Enrichment Factor (EF) were reported to capture early retrieval performance. Model selection was based on the highest validation AUROC, and final results were averaged over five-fold cross-validation.

V. Conclusion

We proposed a contrastive framework that combined cross-modal alignment with bilinear interaction modeling to extract drug–pocket relationships from tokenized sequences. The approach delivered state-of-the-art results on Human and BioSNAP datasets and maintained competitive performance on BindingDB. In virtual screening evaluations, it outperformed previous methods on LIT-PCBA, achieving notable improvements in AUROC and BEDROC. These capabilities supported efficient pre-screening using accessible one-dimensional sequences augmented with novel structure-aware representations.

VI. Acknowledgements

This work was supported by an internal grant from The Hong Kong Polytechnic University (Project No. P0051278, Jung Sun Yoo) and the General Research Fund (Project No. PolyU 15101422, Jung Sun Yoo) from the Research Grants Council of the Hong Kong Special Administrative Region, China.

References

[1] R. A. Copeland, "The drug–target residence time model: a 10-year retrospective," *Nature Reviews Drug Discovery*, 2016.
[2] D. M. York, "Modern alchemical free energy methods for drug discovery explained," *ACS Physical Chemistry Au*, 2023.
[3] B. Zdrazil, "Fifteen years of ChEMBL and its role in cheminformatics and drug discovery," *Journal of Cheminformatics*, 2025.
[4] C. Zhang *et al.*, "BioLiP2: an updated structure database for biologically relevant ligand–protein interactions," *Nucleic Acids Research*, 2024.
[5] T. Liu *et al.*, "BindingDB in 2024: a FAIR knowledgebase of protein–small molecule binding data," *Nucleic Acids Research*, 2025.
[6] A. Miranda-Escalada *et al.*, "Overview of DrugProt task at BioCreative VII," *Database*, 2023.
[7] M. Krenn *et al.*, "SELFIES and the future of molecular string representations," *Patterns*, 2022.
[8] J. Su *et al.*, "Saprot: Protein language modeling with structure-aware vocabulary," *bioRxiv*, 2023.
[9] A. Yüksel *et al.*, "SELFormer: Molecular representation learning via SELFIES language models," 2023.
[10] Z. Lin *et al.*, "Language models of protein sequences at the scale of evolution enable accurate structure prediction," *bioRxiv*, 2022.
[11] W. Ahmad *et al.*, "Chemberta-2: Towards chemical foundation models," 2022.
[12] H. Touvron *et al.*, "Augmenting convolutional networks with attention-based aggregation," *arXiv*, 2021.
[13] P. Bai *et al.*, "Interpretable bilinear attention network with domain adaptation improves drug–target prediction," *Nature Machine Intelligence*, 2023.
[14] M. Zitnik *et al.*, "BioSNAP datasets: Stanford biomedical network dataset collection," http://snap.stanford.edu/biodata.
[15] H. Liu *et al.*, "Improving compound–protein interaction prediction by building up highly credible negative samples," *Bioinformatics*, vol. 31, no. 12, pp. i221–i229, 2015.
[16] L. Chen *et al.*, "TransformerCPI: improving compound–protein interaction prediction by sequence-based deep learning with self-attention mechanism and label reversal experiments," *Bioinformatics*, 2020.
[17] V.-K. Tran-Nguyen *et al.*, "Lit-PCBA: an unbiased data set for machine learning and virtual screening," *Journal of Chemical Information and Modeling*, 2020.
[18] D. Rogers *et al.*, "Extended-connectivity fingerprints," *Journal of Chemical Information and Modeling*, 2010.
[19] D. Cao *et al.*, "propy: A tool to generate various modes of Chou's PseAAC," *Bioinformatics*, 2013.
[20] M. Tsubaki *et al.*, "Compound–protein interaction prediction with end-to-end learning of neural networks for graphs and sequences," *Bioinformatics*, vol. 35, 2019.
[21] I. Lee *et al.*, "DeepConv-DTI: Prediction of drug–target interactions via deep learning with convolution on protein sequences," *PLoS Computational Biology*, 2019.
[22] T. Nguyen *et al.*, "GraphDTA: Predicting drug–target binding affinity with graph neural networks," *Bioinformatics*, 2021.
[23] K. Huang *et al.*, "MolTrans: Molecular interaction transformer for drug–target interaction prediction," *Bioinformatics*, 2021.

[24] R. Spitzer *et al.*, "Surflex-Dock: Docking benchmarks and real-world application," *Journal of Computer-Aided Molecular Design*, 2012.
[25] T. A. Halgren *et al.*, "Glide: a new approach for rapid, accurate docking and scoring. 2. enrichment factors in database screening," *Journal of Medicinal Chemistry*, 2004.
[26] X. Zhang *et al.*, "Planet: A multi-objective graph neural network model for protein–ligand binding affinity prediction," *bioRxiv*, 2023.
[27] M. Brocidiacono *et al.*, "BigBind: Learning from non-structural data for structure-based virtual screening," *arXiv*, 2022.
[28] B. Gao *et al.*, "Drugclip: Contrastive protein–molecule representation learning for virtual screening," in *NeurIPS*, 2023.
[29] C. Cortes *et al.*, "Support-vector networks," *Machine Learning*, 1995.
[30] T. K. Ho, "Random decision forests," in *Proc. ICDAR*, 1995.
[31] H. Zhang *et al.*, "A cross-field fusion strategy for drug-target interaction prediction," *arXiv preprint arXiv:2405.14545*, 2024.
[32] A. T. McNutt *et al.*, "GNINA 1.0: molecular docking with deep learning," *Journal of Cheminformatics*, 2021.
[33] H. Öztürk *et al.*, "DeepDTA: deep drug–target binding affinity prediction," *Bioinformatics*, 2018.